Thermal Balance and Water Ice Sublimation on the Surface of Hyperactive Comet 103P/Hartley2

Yuxian Yue[1], Jiancen Liu[1], and Xiaohui Wang[1]

[1]Beihang University

November 22, 2022

Abstract

Hyperactive comets have attracted attention due to their high water production rate with an unclear mechanism, though some hypotheses are proposed to explain it. Based on the thermal theories of the comet nuclei, this paper studied a comet surface thermal model considering the sublimation of H_2O. In this paper, a method for solving the sublimation rate of water ice by infrared spectra is proposed. The method adopts the assumption of comet nucleus surface temperature roughness and uses the numerical solution of the Fredholm equation. We use the HRI-IR spectra (1.05-4.8 µm) data by EPOXI to analyze the pixel water sublimation rate of hyperactive comet 103P/Hartley2. The results show that the sublimation exists in most areas of the surface with or without surface roughness, and most of the water production rate (70% ~ 90%) may come from the comet nucleus. According to the sublimation law, it is estimated that the sublimation temperature of water ice on 103P is above 180K. If the dust-to-ice volume ratio is 3:1, the sublimation temperature is about 200-210K, which indicates that the water ice may sublimate underneath. This may explain why exposed water ice on the surface cannot be observed while the active fraction of this comet is up to 100%.

Hosted file

essoar.10511051.1.docx available at https://authorea.com/users/532976/articles/598061-thermal-balance-and-water-ice-sublimation-on-the-surface-of-hyperactive-comet-103p-hartley2

Thermal Balance and Water Ice Sublimation on the Surface of Hyperactive Comet 103P/Hartley2

Yuxian Yue*[1], Jiancen Liu[1], Xiaohui Wang[1]

[1]School of Astronautics, Beihang University, Beijing, China.

Corresponding author: Yuxian Yue (sy1715318@buaa.edu.cn)

Key Points:

- This paper shows that water ice sublimation has a significant effect on the surface thermodynamic equilibrium of comet nuclei.

- This paper proposes a new understanding of the high water production rate observed on hyperactive comets.

- Methods of spectral fitting and analysis are applied, including a solution to the Fredholm equation in black-body radiation inverse problem.

Plain Language Summary

This paper analyzed the effect of water ice sublimation on the surface thermal balance of 103P comet nucleus. According to the roughness model and the law of water ice sublimation, the water production rate and water ice sublimation temperature on the comet nucleus surface are inferred.

19   **Abstract**

20   Hyperactive comets have attracted attention due to their high water production rate with
21   an unclear mechanism, though some hypotheses are proposed to explain it. Based on the thermal
22   theories of the comet nuclei, this paper studied a comet surface thermal model considering the
23   sublimation of H_2O. In this paper, a method for solving the sublimation rate of water ice by
24   infrared spectra is proposed. The method adopts the assumption of comet nucleus surface
25   temperature roughness and uses the numerical solution of the Fredholm equation. We use the
26   HRI-IR spectrum (1.05-4.8 μm) data by EPOXI to analyze the pixel water sublimation rate of
27   hyperactive comet 103P/Hartley2. The results show that sublimation exists in most areas of the
28   surface with or without surface roughness, and most of the water production rate (70% ~ 90%)
29   may come from the comet nucleus. According to the sublimation law, it is estimated that the
30   sublimation temperature of water ice on 103P is above 180K. If the dust-to-ice volume ratio is
31   3:1, the sublimation temperature is about 200-210K, which indicates that the water ice may
32   sublimate underneath. This may explain why exposed water ice on the surface can hardly be
33   observed while the active fraction of this comet is up to 100%.

34   **1 Introduction**

35   **1.1 Theory of comet nucleus**

36   According to the comet nucleus theory proposed by Whipple et al. (1951) and studies of
37   an uncounted number of researchers, the volatiles (mainly water ice, dry ice, and other oxides
38   represented by NO_x) on the surface of the comet nucleus sublimates rapidly when the comet
39   moves close to the sun, causing the refractory dust particles to escape, thus forming coma and
40   tail structures. Huebner et al. (2006) systematically summarized the physical characteristics of
41   the comet nucleus, providing a nucleus model and theoretical basis for subsequent researches.
42   The sublimation of volatiles significantly affects the thermal balance on the surfaces of cometary
43   nuclei, since the sublimation rate of the fusible solid is very sensitive to temperature in extremely
44   low gas pressure. The academic has been studying how the volatiles sublimate.

45   Squires and Beard (1961) first studied the thermal balance of the comet nuclei and
46   proposed a method for the study of surface thermodynamics. Following this theory, a series of
47   studies about the thermodynamics of comet nuclei are carried out by many researchers (e.g.,
48   Weissman et al., 1981; Kührt, 1981; Prialnik, 1989; Julian et al., 2000; Gutierrez et al., 2001).
49   The matter stage change and gas flow on the comet nucleus dominated by the thermodynamic
50   state is also widely studied (e.g., Fanale et al., 1984; Benkhoff et al., 1996; Gortsas et al., 2011;
51   Keller et al., 2015; Hu et al., 2017).

52   Lebofsky et al. (1986) proposed the Standard Thermal Model (STM) based on solar
53   radiation and black body radiation which is widely used in planetary science. Spencer et al.
54   (1989) proposed the concept of the thermal inertia of small celestial bodies based on STM and
55   the surface heat conduction model of small celestial bodies, including the comet nuclei.
56   Considering the sublimation of volatiles (mainly water ice) on the comet nuclei, Groussin et al.
57   (2004) established a simplified water ice fraction model, assuming that the nucleus is an ideal
58   sphere and the thermal inertia is zero. Following this model, Groussin et al. (2007,2013), and
59   Davidsson et al. (2009,2012,2015) measured the brightness temperature of 9P, 103P using the
60   Deep Impact and EPOXI near-infrared spectrometer data, as well as 67P and some asteroids
61   from Rosetta, and proposed the concept of surface roughness parameter (the anisothermal

62 parameter) to describe the difference between the brightness temperature spectra and the
63 observed spectra of the nuclei. However, the relationship between the temperature roughness
64 caused by the surface topographic roughness and the sublimation of volatiles on the comet
65 nucleus remains to be studied.

66 **1.2 Hyperactive comet 103P/Hartley2**

67 Comet 103P/Hartley2 is characterized by its small comet nucleus (average radius ~ 600m)
68 and high water production rate (~ 10^{28} molec/s at 1.06 AU), attracting the attention of researchers.
69 According to the approximate model of Groussin et al. (2004), the active area fraction of water
70 ice on its surface is up to ~ 100%. This kind of comet with a high theoretical active fraction is
71 called hyperactive comet by the community. However, when the EPOXI spacecraft visited this
72 comet in 2010, exposed water ice is hardly detected on its surface (A'Hearn et al., 2011), which
73 challenges some established models and assumptions, and brings new discussions.

74 Meech et al. (2011) estimated that more than 90% of the Hartley 2 water originates from
75 extended sources in the coma according to the high water-ice fraction surface model. An icy dust
76 theory was then postulated by Fougere et al. (2013) to explain its high water production rate,
77 suggesting that water is mainly sublimated from pure ice grains in the coma. The model
78 proposed by Kelley et al. (2013) shows that the water production rate brought by pure ice
79 particles with a radius of 30cm is estimated to be 0.03-0.2% of the total water production rate of
80 comets, while this proportion is 30-200% for loose icy dust bulks with a radius up to 4m.
81 Protopapa et al. (2014) derived a lower limit of the sublimation rate from the icy dust particles in
82 the inner coma about 0.00046±0.00001 kg/s with unknown particle size. Whether the water is
83 mainly sublimated from icy dust is still uncertain.

84 On the other hand, Bonev et al. (2013) suggested that there are two sources of gaseous
85 water in the inner coma based on the observed thermal state of water vapor, which indicated that
86 no more than 20% of water is sublimated from icy grains. Harker et al. (2018) also showed that
87 the main component of 103P's dust particles is amorphous materials mainly composed of carbon,
88 and no direct evidence of water ice in the dust was found. Yue et al. (2021) performed a dynamic
89 simulation on the spatial distribution of 103P's dust coma. Their results show that the large-scale
90 spatial distribution of comet dust is hardly affected by water ice sublimation. More recent
91 research by Protopapa et al. (2021) also suggested that there is no evidence for the existence of
92 water-ice grains in the coma of another hyperactive comet, 46P/Wirtanen, based on ground-
93 based observations.

94 All those results indicate that the water ice grains ejected into the coma may not be the
95 only reason for the hyperactivity of some comets. The "hyperactive" nature of 103P is yet to be
96 fully understood.

97 **1.3 A new method: fitting sub-pixel temperature by solving inverse problem of black**
98 **body radiation**

99 This paper reconstructed the thermodynamic model and analysis of 103P following
100 Groussin et al.'s research (2004 and 2009), using the HRI-IR (High Resolution Instrument -
101 InfraRed) data from EPOXI(DIXI) mission.

102 In this paper, the assumption of temperature roughness is adopted, and the distribution of
103 sub-pixel surface temperature of 103P is fitted using the infrared spectral data. This fitting is a
104 typical inverse problem of black body radiation, which has been systematically studied by

105 Bojarsky (1982), Chen et al. (1990), Dai et al. (1992) and numerically solved by Ji et al. (2006,
106 2011). In this paper, the Fredholm integral equation, the core equation of the problem, is solved
107 by using the basis function fitting method, and the approximate distribution of the temperature in
108 the sub-pixel level is obtained. Using this distribution, the energy absorbed by the sublimation of
109 water ice on the surface can be calculated based on the energy balance equations, and the
110 corresponding surface sublimation rate can then be obtained.

111 The total water production rate of the comet nucleus can be obtained by integrating the
112 surface water sublimation rate. At the same time, the relationship between water ice volume ratio
113 (according to dust-to-gas ratio) and sublimation temperature can also be established based on the
114 gas law, and the actual sublimation temperature of water ice on 103P surface can be inferred.

115 This study considers the 3-D shape and dynamic model of the nucleus. The shape model
116 is from the research of Thomas et al. (2013) and the rotation model is from Belton et al. (2013).
117 The DEM is from Farnham et al. (2012).

118 **2 The thermal model on the comet nucleus surface**

119 Based on the thermodynamic model of the surface of a small celestial body by Spencer et
120 al. (1989), the surface of the small celestial body satisfies the one-dimensional conductive heat
121 flow equation when there is no volatile sublimation:

$$\rho C \frac{\partial T(x,t)}{\partial t} = \frac{\partial}{\partial x}\left(\kappa \frac{\partial T(x,t)}{\partial x}\right) \tag{1}$$

122 Where T is temperature, x is surface depth, t is time, ρ is density, C is specific heat
123 capacity, and κ is thermal conductivity.

124 The thermal balance of the surface point (x=0) is considered to be mainly determined by
125 solar radiation (considering albedo), black-body radiation, and heat conduction. Therefore the
126 boundary condition on the surface is:

$$\left(\kappa \frac{\partial T(x,t)}{\partial x}\right)_{x=0} = \varepsilon\sigma T^4(0,t) - (1-A)F_S(t) \tag{2}$$

127 Where A is the bolometric Bond albedo, and F_s is the time-dependent flux of incident
128 sunlight. σ is the Stefan-Boltzmann constant. ε is the bolometric emissivity.

129 For a surface that experiences periodic heat input, such as the surface of a rotating
130 cometary nucleus, the periodic temperature variation decreases exponentially with respect to
131 depth. The thermal skin depth (Wesselink et al., 1948), d, represents the depth of an e-fold
132 decrease in temperature variation. The second boundary condition is at infinite depth where the
133 temperature gradient is 0, i.e. no heat flow. In practice, generally at a depth of D=8d, the heat
134 flow is considered 0:

$$\left.\frac{\partial T(x,t)}{\partial x}\right|_{x=D} = 0 \tag{3}$$

135 With the above boundary conditions, the heat conduction equation can be numerically
136 integrated, and the variation of the temperature on the surface over time can be obtained. This
137 variation is related to a coefficient $\Gamma=(\kappa\rho C)^{0.5}$, termed thermal inertia.

138   For asteroids without sublimation, the STM (standard thermal model) proposed by
139   Lebofsky and Spencer (1989) can be used to establishing the surface thermal model. Considering
140   an asteroid with a flat surface, the thermal balance (in W/m²) of the surface can be as

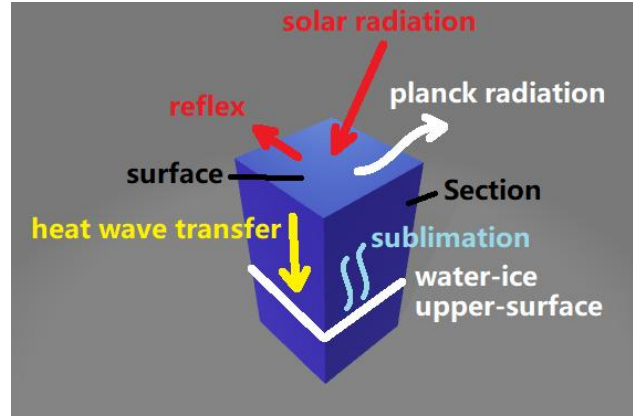$$I_{sun} = I_{REFF} + \dot{E} + P \tag{4}$$

141   In which I_{sun} is the solar radiation, I_{REFF} is the reflex (mainly decided by Bond albedo), $\dot{E}$
142   is the heat conduction efficiency, and P is the Planck radiation of the surface. Because the
143   surface is summed to be flat, P is actually the black-body radiation corresponding to the surface
144   temperature. According to the STM, the thermodynamic model of 103P without water ice
145   sublimation and surface roughness can be established. Figure 1 shows the temperature
146   distribution on the surface based on the DEM of 103P. (The detailed model and data can be
147   found in the repository of this paper.)

148   The thermal inertia Γ is approximated to 50 W/K/m²/s$^{1/2}$ according to Groussin et al.
149   2013's research. The albedo used in the model is 0.04 according to Li et al. (2013) and A' Hearn
150   et al. (2011). The heliocentric distance is 1.06AU.

151
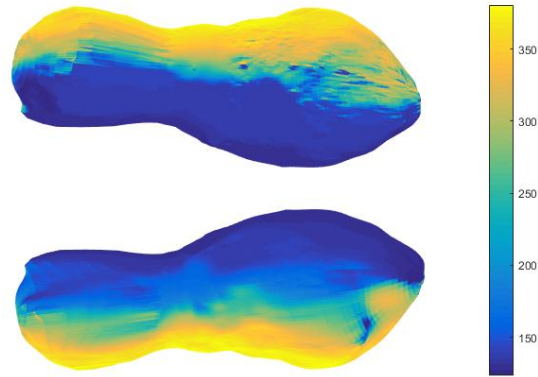
Fig.1 Surface temperature distribution of 103P simulated by the STM (without sublimation)

154   In fact, the sublimation of water ice on the comet nucleus will affect the thermodynamic
155   process on the surface. According to the analysis of jet areas on the surface of 103P (Shi et al.,
156   2016; Hu et al., 2017; Herny et al., 2021) and surface data of comet 67P from Rosetta
157   (Davidsson et al., 2022, Groussin et al., 2019, Bouquety et al., 2021, Fornasier et al., 2016, De
158   Sanctis et al., 2015), water ice may exist at a certain depth in the surface layer of the comet
159   nucleus. The simplified thermodynamic model of the surface layer of the comet nucleus is shown
160   in Fig.2. This model does not involve the surface roughness (or considers that the surface is
161   small enough to be flat).

162

Fig.2 The simplified model of surface layer of comet nucleus

164 Based on the surface layer model, Eq.(5) can be obtained according to the energy balance
165 (Huebner et al., 2006):

$$I_{sun} = I_{REFF} + \dot{E} + P' + S + E_g \tag{5}$$

166 In which I_{sun} is the solar radiation, I_{REFF} is the reflex (mainly decided by Bond albedo), $\dot{E}$
167 is the heat conduction efficiency, and P' is the actual black-body radiation of the surface with
168 temperature roughness. S is the energy absorbed by sublimation of volatiles (mainly water ice in
169 most areas), E_g is the heat absorption of water vapor. S and E_g include the energy of the possible
170 re-condensation/re-sublimation.

171 For water ice, under low temperature (<300K) and low pressure (<1kPa), the energy
172 changes between solid crystalline phases are always low as about 1.94 kJ/kg (McMillan et al.,
173 1965, Yamamuro et al., 1987, Handa et al., 1988), while the energy absorbed by sublimation is
174 about 2830 kJ/kg (Feistel et al., 2007), so S can be approximated as sublimation energy.

175 At the same time, the specific heat capacity of water vapor (under constant pressure) is
176 about 1.78 kJ/kg/K/m^2（"Pure Component Properties" (Queriable database). Chemical
177 Engineering Research Information Center. Retrieved 8 May 2007.），which is only about 170
178 kJ/kg when the temperature of water vapor is raised by 100K. Eg is also far less than S and can
179 be omitted.

180 Therefore, the sum of S and E_g can be approximately replaced by the sublimation term:

$$S + E_g \approx \omega \cdot H \tag{6}$$

181 In which ω is the water ice sublimation rate from unit area surface layer, and H is the
182 latent heat of water ice sublimation, which is nearly a constant between 100-300K, taken as
183 2830kJ/kg (Feistel et al., 2007) in our modeling.

184 Comparing Eq.(4) and Eq.(5), it can be seen that the difference between the surface
185 black-body radiation P based on the STM and the actual surface radiation P' is mainly caused by
186 the sublimation term:

$$P = P' + S + E_g \approx P' + \omega \cdot H \tag{7}$$

187   Therefore, when the theoretical radiation P has been determined according to the
188 NEATM, the sublimation rate ω can be approximately calculated as long as the actual black-
189 body radiation *P'* on the surface of the comet nucleus is obtained.

3 Process of infrared data of 103P nucleus from EPOXI mission

191   The Deep Impact spacecraft has provided infrared measurements of 103P using an HRI-
192 IR (1.05–4.8 μm) spectrometer instrument (High Resolution Instrument-InfraRed spectrometer;
193 Hampton et al., 2005). During the DIXI (Deep Impact eXtended Investigation), the Deep Impact
194 spacecraft flies by 103P/Hartley 2 at the closest approach distance of 700 km on 4 November
195 2010, collecting data from this hyperactive comet. The infrared data of 103P is calibrated in 3
196 versions (v1.0, v2.0, and v3.0)(NASA.PDS: small bodies: EPOXI, https://pds-
197 smallbodies.astro.umd.edu/data_sb/missions/epoxi/index.shtml. Version 3.0 includes the
198 application of scaled master dark subtraction for DOY 307 and in scene dark subtraction for
199 DOY 311-313, as well as the use of an average per scan optical bench temperature in the pipeline
200 processing. Version 3 also includes the calibration enhancements implemented in Version 2 of
201 this dataset: a new per-pixel linearity correction treatment and its propagation through the
202 calibration steps (i.e., bad-pixel maps, flat-field file update, revised spectral calibration curve),
203 new mode-dependent master darks, an optimized scaling factor for the master dark, and a
204 refinement in the absolute spectral calibration curve (McLaughlin et al., 2014).

205   In this paper, the surface thermodynamic state of 103P was studied by using the infrared
206 spectral data V3.0.

3.1 Hypothesis

208   According to the model in Section 2.1 and the research on surface roughness by Groussin
209 et al. (2009, 2013) and Davidsson et al. (2009, 2012, 2015), we give the following assumptions:
210 (in the single-pixel area corresponding to the observation data)

211   **Hypothesis-1:** There is temperature roughness on the comet nucleus surface, and the
212 fraction of the area with temperature T in a pixel area is assumed to be $g(T)$. The integral of $g(T)$
213 under all temperatures is 1, so it can be regarded as a probability density function (PDF). Note
214 that this surface refers to the surface area corresponding to the observation projection plane. The
215 pixel thermal radiation of the nucleus surface observed by HIR-RI is inverse black body
216 radiation.

217   **Hypothesis-2:** For areas with solar radiation, there is a theoretical upper limit on the
218 surface temperature of the comet nucleus. The maximum temperature is the corresponding black-
219 body radiation temperature (no sublimation) under direct sunlight (I_{sun0}) considering the surface
220 roughness, set as T_H:

$$\sigma T_H{}^4 = I_{sun0} \tag{8}$$

221   Where σ is the Stefan-Boltzmann constant. For 103P at a distance of 1.06 AU from the
222 sun, T_H is about 382K. Note that the incidence angle of the small region corresponding to T_H is
223 0°, so there is hardly self-heating effect in theory. The maximum temperature fitted in the study
224 of Groussin et al. 2013 also does not exceed 370K, so it is reasonable to take 382k as the upper
225 limit of the theoretical temperature.

226   **Hypothesis-3:** For areas receiving solar radiation, there is a lower limit for the surface
227 temperature. The minimum temperature corresponds to areas with no sunshine and the water ice
228 coverage reaches 100%. Therefore, the minimum temperature T_L is set as the temperature of
229 water ice sublimation (200K, Hubner et al., 2006).

230   **3.2 Data fitting**

231   The pixel infrared spectrum of 103P is mainly composed of reflection spectrum and
232 black-body radiation spectrum:

$$F(\lambda) = F_{REFF}(\lambda) + \varepsilon_d \cdot u(\lambda) \tag{9}$$

233   Where F is the direct observed spectrum, F_{REFF} is the reflection spectrum, ε_d is the
234 directional emissivity, and u is the black-body radiation spectrum with sub-pixel temperature
235 roughness.

236   According to Kirchhoff's law, the directional emissivity ε_d of an isotropic scatter can be
237 derived from the reflectance factor *REFF* (Hapke, 1993):

$$\varepsilon_d = 1 - REFF = 1 - \frac{\pi F_{REFF}(\lambda)}{F_{receive}(\lambda)} = 1 - \frac{\pi F_{REFF}(\lambda)}{\cos(i) F_{sun}(\lambda)/r_h^2} \tag{10}$$

238   Where $F_{receive}$ is the received irradiance from the sun, i is the incidence angle, F_{sun} is the
239 solar irradiance at 1 AU, and r_h is the heliocentric distance of the comet at the time of
240 observation (1.06 AU for 103P).

241   F_{REFF} can be approximately modeled as the solar spectrum with a spectral slope S′ (in %
242 per kÅ and derived in the spectral range1.5–2.2 μm) and normalized to the data at 1.8μm
243 (Groussin et al., 2013).

244   As the observation band is limited in 1.05-4.8 μm, it is not easy to accurately fit the
245 surface temperature distribution corresponding to the pixel through $u(\lambda)$. According to the
246 assumption in Section 2.2.1, $u(\lambda)$ is actually a mixed spectrum of different temperatures with
247 different area ratios (the same assumption is also made in Davidsson et al., 2015). Therefore, the
248 pixel-level $u(\lambda)$ is:

$$u(\lambda) = \int_0^\infty g(T)B(\lambda,T)dT \tag{11}$$

249   Where $g(T)$ is the temperature distribution function (assumption 1 in Section 2.2.1), and
250 B is the ideal black-body radiation. Considering hypothesis-2 and hypothesis-3 in Section 2.2.1,
251 the upper and lower limits of T are T_H and T_L, respectively, then (11) becomes (11'):

$$u(\lambda) = \int_{T_L}^{T_H} g(T)B(\lambda,T)dT \tag{11'}$$

252   In this formula, u is the known data, B is the known function, and only $g(T)$ needs to be
253 solved. This is a typical inverse problem of black-body radiation. Equation (11') is a typical
254 Fredholm integral equation of the first kind and can be solved by numerical method. According
255 to the research of (Ji et al., 2006, 2011), we use the method of basis function fitting. Since the
256 function type of $g(T)$ is also unknown, we choose the piecewise function (the Floor Function)
257 with unknown parameters as the approximate distribution function, as shown in Fig.3.

258
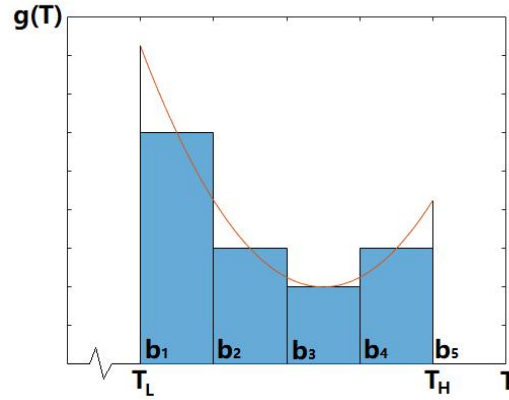
Fig.3 The Floor Function was used to fit the temperature distribution function. The horizontal axis is the temperature and the vertical axis is the probability density. The red curve in the figure is the actual distribution of *T*, and the blue function is the fitted distribution.

To balance the accuracy of fitting results and the calculation complexity, we choose the 4-floors distribution to fit $g(T)$. Considering the characteristics of the Planck function, the five boundary points of the 4 floors are:

$$b_1 = T_L;$$

$$b_2 = \sqrt[4]{\frac{T_H^{\,4} - T_L^{\,4}}{4} + T_L^{\,4}};$$

$$b_3 = \sqrt[4]{2 \cdot \frac{T_H^{\,4} - T_L^{\,4}}{4} + T_L^{\,4}}; \qquad (12)$$

$$b_4 = \sqrt[4]{3 \cdot \frac{T_H^{\,4} - T_L^{\,4}}{4} + T_L^{\,4}};$$

$$b_5 = T_H.$$

266

The approximated distribution function of *T* is:

$$g(T)_{appr} = \begin{cases} \dfrac{x_1}{b_2 - b_1}, & T \in [b_1, b_2) \\[2mm] \dfrac{x_2}{b_3 - b_2}, & T \in [b_2, b_3) \\[2mm] \dfrac{x_3}{b_4 - b_3}, & T \in [b_3, b_4) \\[2mm] \dfrac{x_4}{b_5 - b_4}, & T \in [b_4, b_5] \end{cases} ; \qquad (13)$$

$$x_1 + x_2 + x_3 + x_4 = 1.$$

267   In fact, the anisothermal parameter $Λ$ which takes into account the fact that the surface is
268   rough at the sub-pixel scale (Davidsson et al., 2009, Groussion et al., 2009, 2013) means using a
269   two-points distribution model (T_{color} is one point and 0K is another point) to fit $g(T)$, and the area
270   fraction of T_{color} is the parameter $Λ$:

$$g(T)_{appr'} = \begin{cases} Λ, T = T_{color} \\ 0, T \neq T_{color} \end{cases} \tag{14}$$

271   The proposal of anisothermal parameter $Λ$ determines the existence of temperature
272   roughness, but taking 0K as one temperature distribution point is not accurate. Therefore, the 4-
273   floors distribution fitting method proposed in this paper is actually an improvement based on the
274   rationality of the hypothesis.

275   We used the HRI-IR data of version 3.0 (5001004a, b, and 5005001) for fitting, and
276   obtained the temperature distribution of effective pixels. Figure 4 shows the fitting spectrum and
277   physical information of two sampled pixels.


278
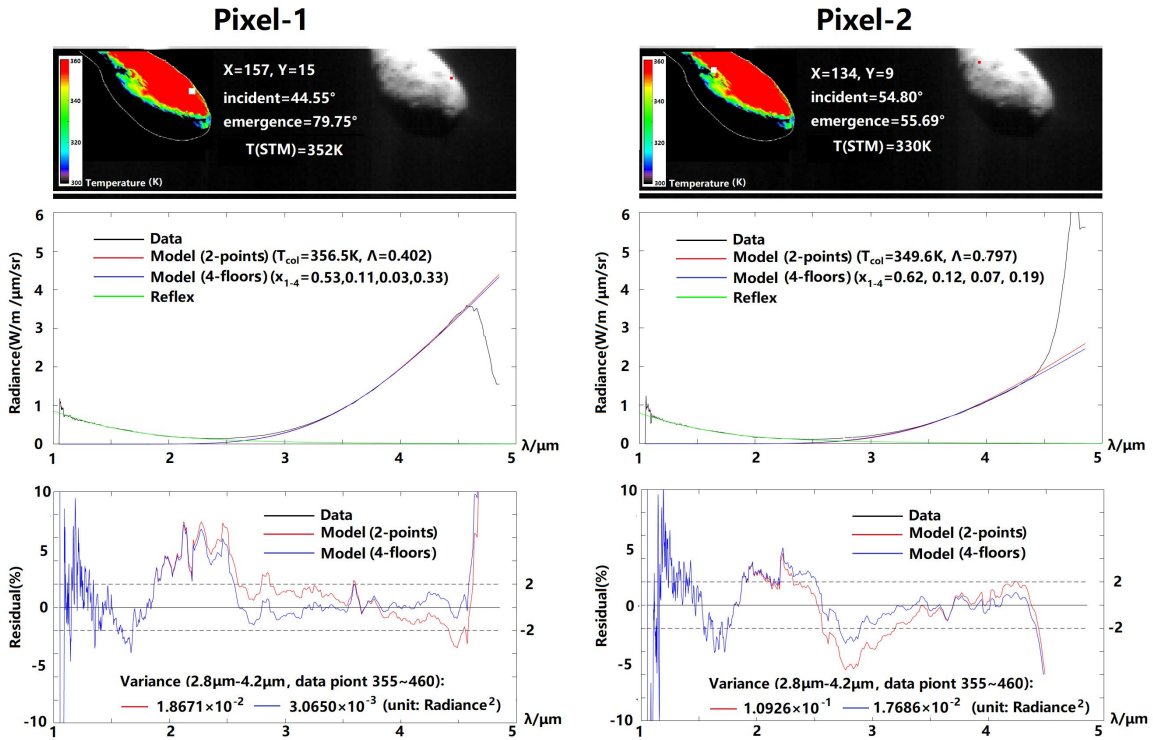
Fig.4 The spectra fitting. The left penal is pixel (15,157) and the right penal is pixel (9,134).
Both pixels are from data 5001004. The top floor is the location of the pixel, the red point
on the HRI-IR image (right, in 3.2 µm), and the white point on the STM temperature
simulation image (left). The second floor is the fitting spectra. The third floor is the related
error of the fitting. In the figure, the black curve is the observed spectra, the red curve is
the fitted spectra by the 2-points model, and the blue curve is the fitted spectra by the 4-
**floors function model.**

286   In most effective pixels, the spectrum fitted by the 4-floors method has smaller residuals
287   (as well as variance) compared to that fitted by the 2-points method, while the approximate limit
288   of residuals of both methods is about ±2%.

289   In order to study the effect of water ice sublimation on the surface spectrum, we also
290   simulated the theoretical radiation spectrum without water ice sublimation. This spectrum
291   assumes surface roughness and is derived using the surface model from Davidsson et al., 2015.
292   The spectrum is simulated based on the incident angle, emergence angle, and azimuth angle of
293   each pixel, using a Gaussian random roughness model with different roughnesses (5°, 20°, and
294   35° in Fig.5). Using this model, the theoretical radiation spectrum of each pixel without
295   sublimation under different roughness can be obtained. It is compared with the spectrum fitted to
296   the observation data to see how sublimation affects the surface spectrum (Fig. 6).

297
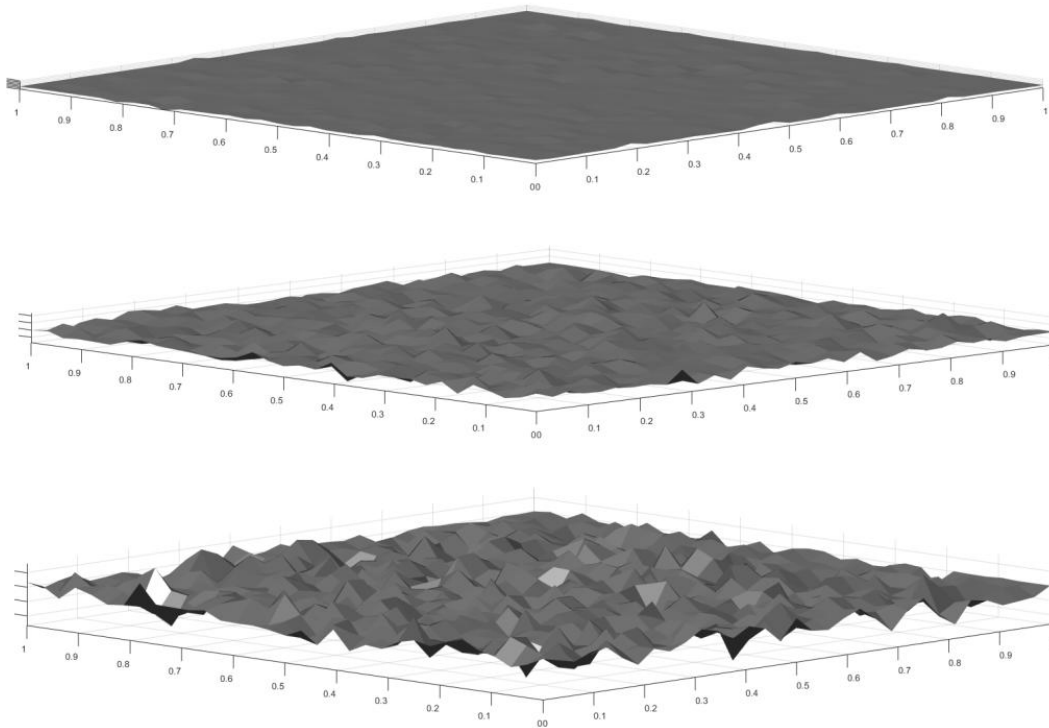
**Fig.5 Surface roughness model used in this study. The model adopted Gauss random
roughness and simulated 1024 facets per unit area (m^2). The roughness of the three
simulated surfaces in the figure is 5°, 20°, and 35° from top to bottom.**

301

302
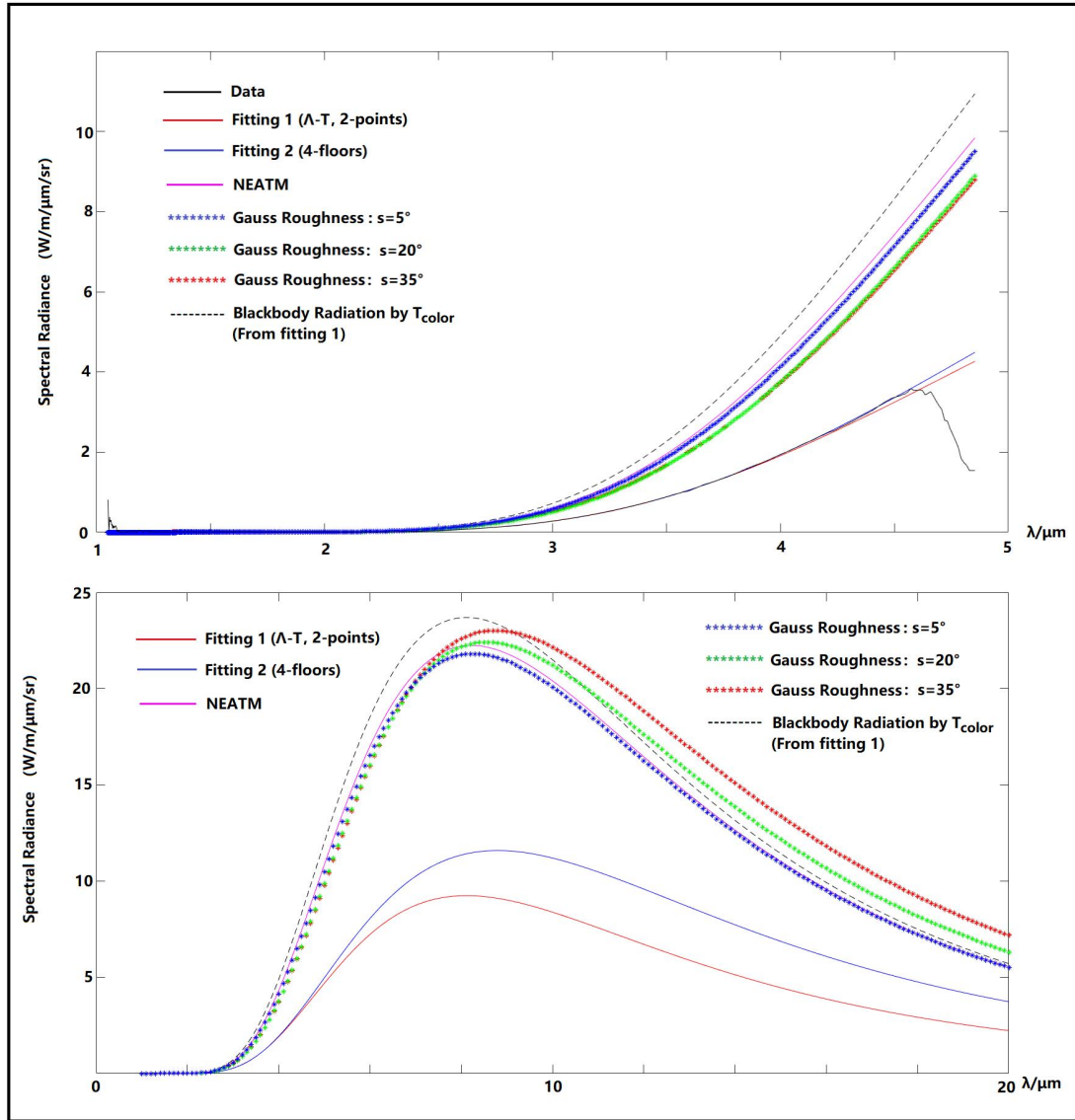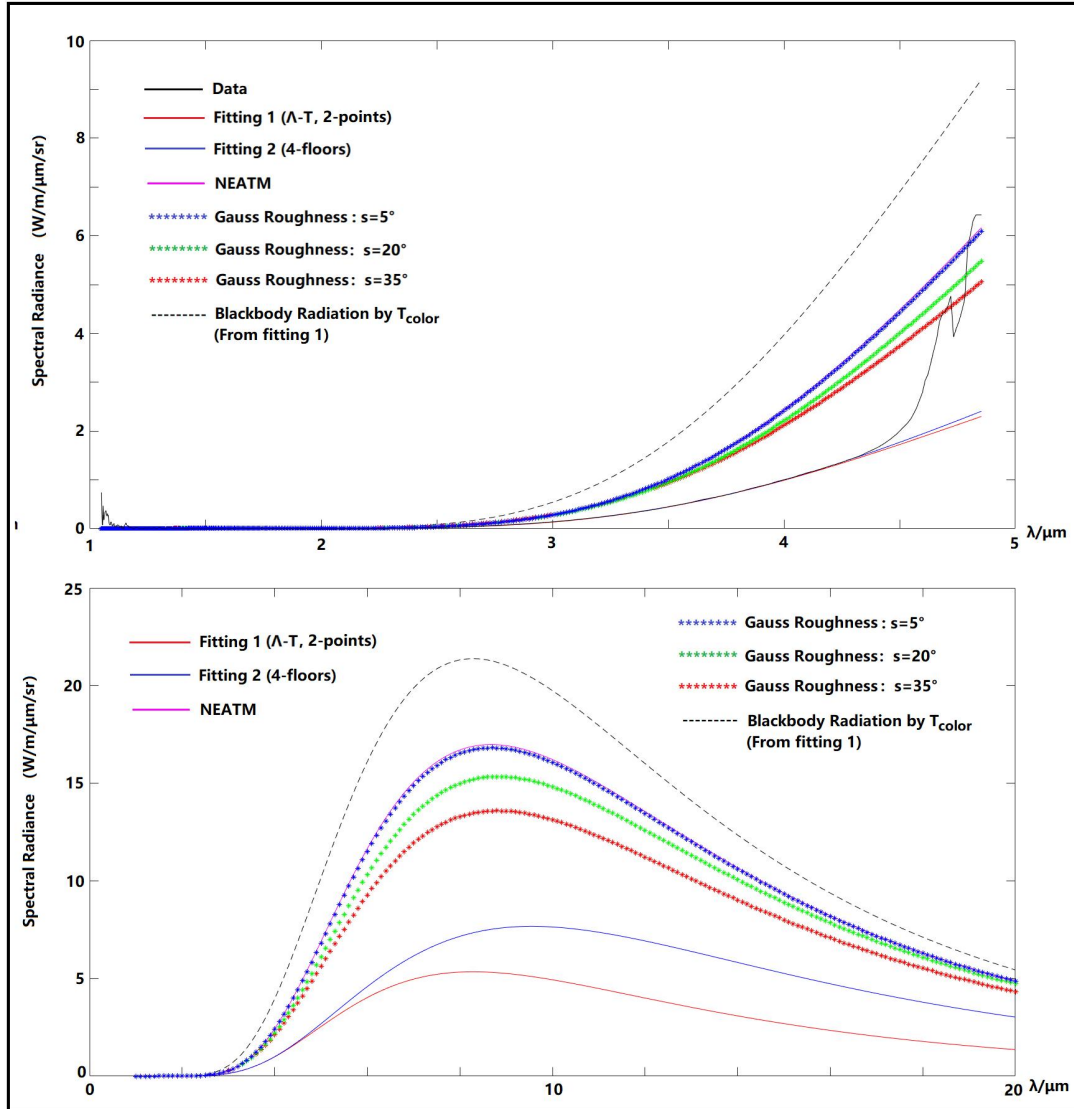
Fig.6(a,b) Spectrum only considering the surface roughness and spectrum fitted to the observed data. The first box is Pixel-1 (15,157) in Fig.4, and the second box is Pixel-2 (9,134). In each box, the upper panel is in 1-5μm, and the lower panel is in 0-20μm. In this figure, the red curve is the fitted spectrum obtained by the two-points method, the blue curve is the fitted spectrum obtained by the 4-floors method, the black curve is the observed spectrum. The purple curve is the STM model spectrum without considering the surface roughness nor sublimation. The blue, green and red dotted lines represent the spectrum of non-sublimation surfaces with roughness of 5°, 20°, and 35°, respectively. The black dashed line is the black body radiation spectrum corresponding to the fitted color temperature in the study of Groussin et al. (2013).

The surface roughness has a non-negligible influence on the real spectrum. However, based on our simulations or Davidsson's 2015 study, the surface roughness of Gauss type (or Fractal type) has an impact on the spectrum within 30%. Compared with the above simulations, the reason why the observed spectrum is significantly lower (>60%) than the STM prediction spectrum is likely to be the sublimation of water ice.

318 In other words, both surface roughness and water ice sublimation have a significant
319 impact on the surface spectrum of the comet nucleus. Using the energy difference between the
320 two types of spectrum (with and without sublimation), the energy absorbed by the sublimation of
321 water ice can be calculated, and the relevant parameters can be further obtained.

322 **3.3 Water sublimation rate**

323 After obtaining an accurate temperature distribution in each pixel, we can use the Planck
324 radiation formula to calculate the actual black-body radiation energy integral corresponding to
325 each pixel (integration of the fitting spectrum, Model:4-floors in Fig.6)：

$$P' = \int_0^\infty \int_{T_L}^{T_H} g(T)B(\lambda,T)dTd\lambda = \int_{T_L}^{T_H} g(T)\int_0^\infty B(\lambda,T)d\lambda dT \approx \int_{T_L}^{T_H} g(T)_{appr}\sigma T^4 dT \tag{15}$$

326 While the theoretical black-body radiation obtained by NEATM (integration of the
327 bottom panel, s=5°, in Fig.6) is:

$$P = \sigma T_{NEATM,s}^{\ \ 4} = \int_0^\infty F_{NEATM,s}(\lambda)d\lambda \tag{16}$$

328 Then, according to Eq.(7), i.e. the sublimation efficiency is approximately the difference
329 between P and P':

$$I_{sub} = \omega \cdot H = P - P' \tag{17}$$

330 the water ice sublimation rate ω corresponding to each pixel can be calculated (Fig. 5).

5001004a   5001004b   5005001

331
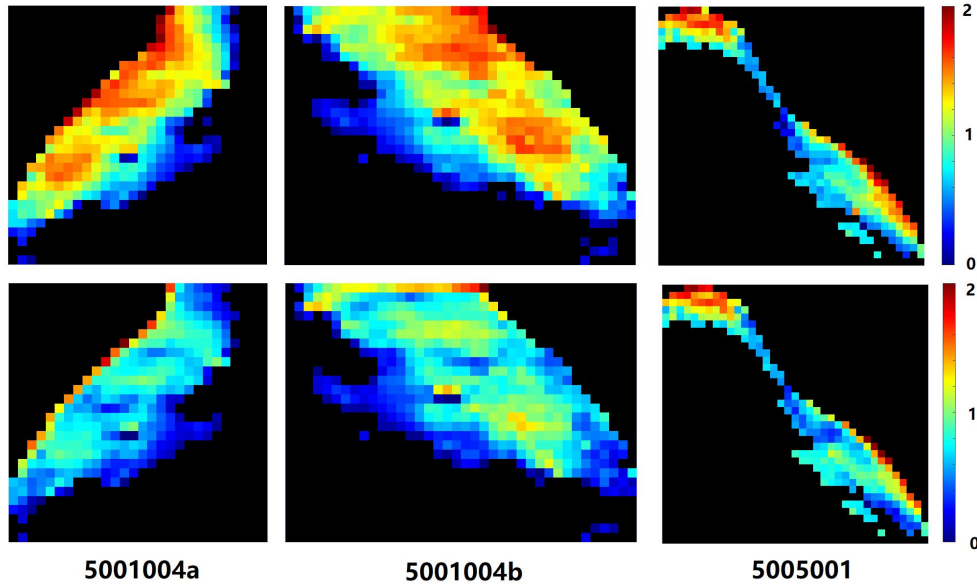
Fig.7 Water ice sublimation rate of the 103P nucleus (modeled surface roughness is 5°).
The upper panel is the result by 2-points distribution fitting (T_{color} and Λ), and the lower
panel is the result by 4-floors distribution fitting. Unit: 10^{-4} kg/s/m².

335 Figure 7 shows that there is significant water ice sublimation in most areas on the surface
336 of the 103P comet nucleus, while areas with smaller incident angles have relatively higher
337 sublimation rates. The active fraction of the comet is up to nearly 100% in day hemisphere,
338 which is consistent with the conclusion in Groussin et al.'s research in 2004.

339   After integrating the sublimation rate of water ice in all effective pixels according to the
340   spectrum (with roughness of 0°,5°,20°and 35°), we get the water production rate of the comet
341   nucleus in the photo (Table.1). The relative error caused by temperature fitting in Section 3.2 is
342   no more than 5% beside the model error.

343   **Table.1 The water production rate from three groups of data (a: 5001004a, b: 5001004b, c:**
344   **5005001) under two fitting methods (2 pionts and 4-floors).Unit: kg/s.**

Data (Method)		a (2-points)	a (4-floors)	b (2-points)	b (4-floors)	c (2-points)	c (4-floors)
Q_{eff} (kg/s)	s=0°	196.2	101.2	146.3	98.3	124.2	109.2
	s=5°	194.8	99.8	144.1	96.1	123.8	108.8
	s=20°	191.2	96.2	138.8	90.8	120.1	105.2
	s=35°	185.1	90.1	131.2	83.2	113.7	98.8
Effective Pixels		354		584		236	
Effective Area		$1.0982×10^6$ m^2		$9.9768×10^5$ m^2		$1.0404×10^6$ m^2	
Area Ratio*		≈0.4192		≈0.3808		≈0.3971	
Q (kg/s)	s=0°	468.0	241.5	384.2	258.1	312.8	275.0
	s=5°	464.7	238.1	378.4	252.4	311.8	274.0
	s=20°	456.1	229.5	364.5	238.4	302.4	264.9
	s=35°	441.6	214.9	344.5	218.5	286.3	248.8
Q/Q_{ob}	s=0°	156.0%	80.5%	128.1%	86.0%	104.3%	91.7%
	s=5°	154.9%	79.4%	126.1%	84.1%	103.9%	91.3%
	s=20°	152.0%	76.5%	121.5%	79.5%	100.8%	88.3%
	s=35°	147.2%	71.2%	114.8%	72.8%	95.4%	82.9%
Error bar *		±20%					

345   *Area ratio refers to the proportion of the area of the daytime hemisphere in the image to the
346   total area of the daytime hemisphere of the comet nucleus (~ 0.5×5.24km^2 = 2.62km^2).

347   *Error bar limit refers to the maximum limit of relative error caused by surface roughness in the
348   model. The data results under different roughnesses are under a low error bar (<20%).

349   This result shows that the water production rate obtained by the 4-floors fitting method is
350   close to the observed total water production rate (~ 300kg/s, A' Hearn et al., 2011; Meech et al.,
351   2011). This indicates that when the hypotheses in Section 2.2.1 are valid, most of the water
352   production of 103P may come from the nucleus surface.

353

4 Water sublimation of the nucleus

In Section 3, the sublimation rate of the comet nucleus surface is already obtained using a 4-floors temperature fitting method. According to the gas sublimation theory, the relationship between sublimation temperature and water ice coverage can be then determined. When the water ice fraction is p_w, the actual areal sublimation rate is:

$$\omega(T) = p_w \cdot \omega_0(T) \tag{18}$$

Where $\omega(T)$ is the actual water ice sublimation rate, ω_0 is the water ice sublimation rate from unit pure water ice area, which is given by Knudsen's law of diffusion (Kramers et al., 1951):

$$\omega_0(T) = p_{st}(T)\sqrt{\frac{M_{gas}}{2\pi RT}} \tag{19}$$

where $p_{st}(T)$ is the saturated vapor pressure, which is given by the formula of Buck et al. (1996) as a function of temperature:

$$p_{st}(T) = \begin{cases} 611.21 \cdot \exp(\dfrac{(18.678 - t/234.5)}{258.14 + t}t), & t > 0 \\ 611.15 \cdot \exp(\dfrac{(23.036 - t/333.7)}{279.82 + t}t), & t < 0 \end{cases}, \quad t = T - 273.15 \tag{20}$$

When $p_w=1$, the lower limit of sublimation temperature T_{lim} can be calculated according to Eq.(18-20), which is the minimum temperature required to maintain the observed water ice sublimation rate, which is about $180 \sim 200$K.

A' Hearn et al. (2011), Dello Russo et al. (2011), Crovisier et al. (2013), Boissier et al. (2013) derived a dust-to-gas ratio of about 2-6. Considering the mass conservation of the comet nucleus, suppose that the water to dust volume ratio is 1:3, the water ice coverage of the volatile layer of the comet nucleus is approximately 0.39. The approximate sublimation temperature T_{appr} calculated under this circumstance is about $200 \sim 210$K. The upper panel of Fig.8 is T_{lim}, and the lower panel is T_{appr}.

5001004a   5001004b   5005001
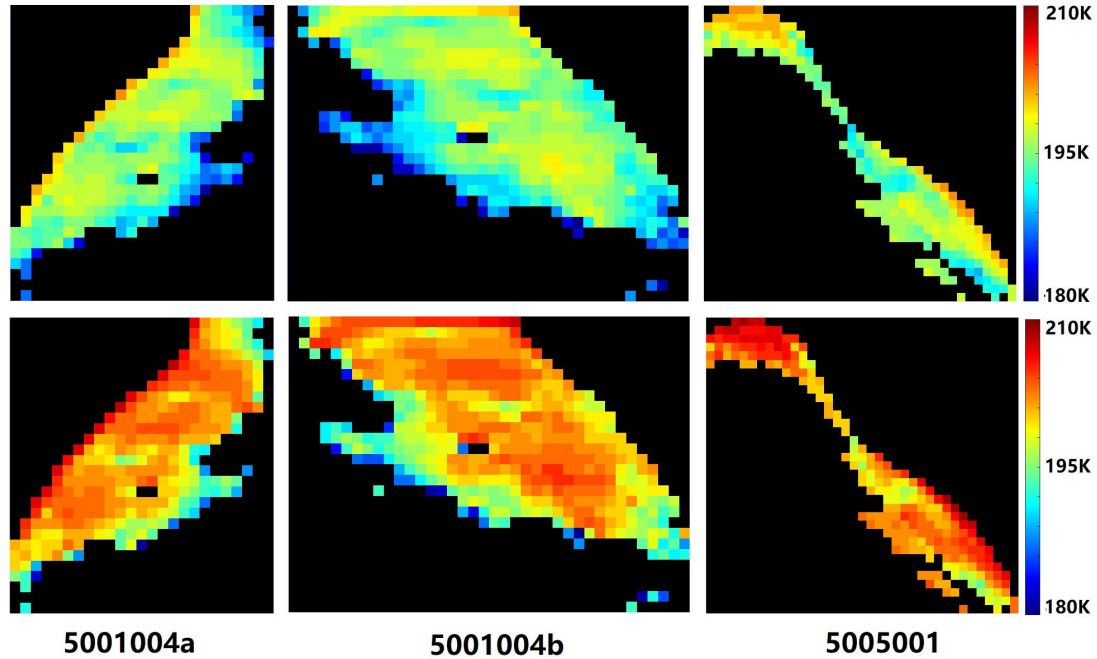
Fig.8 The sublimation temperature of water ice on 103P (surface roughness is 5°). The top panel is the minimum temperature (water ice fraction=1), while the bottom panel is the approximate temperature when the water to dust volume ratio is 1:3(water ice fraction ~0.39). Both panels are derived using the 4-floors temperature fitting method.

Such lower temperatures exist only in the dark areas or under the surface of the comet nucleus. Considering the instability of the dark areas (sometimes being illuminated), this conclusion further indicates that the water on the surface of the comet nucleus is likely to sublimate below the surface of the comet nucleus.

On the one hand, this explanation confirms the surface layer model in Section.2. On the other hand, it also explains why exposed water ice is hardly detected on the surface: most of the water ice is sublimating under the surface quietly, only exposing its existence through the energy loss of the surface infrared spectrum.

5 Conclusions

1. The approximate sub-pixel temperature distribution is solved by using the numerical solution of the inverse black-body radiation problem in this study, and the solution of Fredholm equation is fitted based on the theory of surface roughness proposed by Groussin et al. (2013) and Davidsson et al. (2015). Both surface roughness and water ice sublimation have a significant influence on the surface spectrum.

2. The sublimation rate of water ice on the surface of the comet nucleus is obtained by the energy balance equation and infrared spectrum data from the EPOXI mission. The results show that most of the water production (70% ~ 90%) of comet 103P may come from the surface of the comet nucleus according to the fitted spectrum and the surface roughness model.

396

397   3. Combined with mass conservation, it is calculated that the sublimation temperature of
398 water ice on the 103P nucleus is higher than 180K. Assuming that the comet nucleus is isotropic
399 and the volume ratio of gas to dust is 1:3, the approximate sublimation temperature of water ice
400 on 103P is about 200-210K. Most of the water ice is presumed to sublimate at a certain depth
      underneath.

401

402

420   McLaughlin, S.A., B. Carcich, S.E. Sackett, K.P. Klaasen, L.M. Feaga, and S. Protopapa,

421   EPOXI 103P/HARTLEY2 ENCOUNTER - HRII CALIBRATED SPECTRA V3.0, DIF-

422   C-HRII-3/4-EPOXI-HARTLEY2-V3.0, NASA Planetary Data System, 2014.

423   https://pds-smallbodies.astro.umd.edu/holdings/dif-c-hrii-3_4-epoxi-hartley2-

424   v3.0/dataset.shtml

425   • Thanks：

426   The authors would like to thank the individual efforts and dedicated contributions of the

427   numerous engineers and scientists who were critical in obtaining critical data on Comet 103P.

428   We thank Li-Jianyang and O. Groussin for very helpful discussions and advice.

429

430   **Open Research**

431   The methods used and the results obtained in this paper all are publicly available.

432

433   **References**

434   A'Hearn, M.F. et al., 2011. EPOXI at Comet Hartley 2. *Science*, 332, 1396–1400.

435   Belton, M.J.S. et al., 2013. The complex spin state of 103P/Hartley 2: Kinematics and

436   orientation in space. *Icarus*, 222, 595–609.

437   Benkhoff et al. 1996. Modeling the thermal properties and the gas flux from a porous,

438   ice-dust body in the orbit of P/Wirtanen. *Planetary and Space Science*, 44, 665-673.

439   Boissier, J. et al., 2013. Gas and dust productions of comet 103P/Hartley 2 from

440   millimetre observations: interpreting rotation-induced time variations. *Icarus*, 228, 197-216.

441   Bojarski, N. N. Inverse black body radiation. *IEEE Trans Antennas and*

442   *Propagation*,1982,30(4): 778-780.

443   Bonev, P. B. et al., 2013. Evidence for two modes of water release in Comet

444   103P/Hartley 2: Distributions of column density, rotational temperature, and ortho-para ratio.

445   *Icarus*, 222, 740–751.

446   Bouquety et al., 2021, Ancient and present surface evolution processes in the Ash region

447   of comet 67P/Churyumov-Gerasimenko. *A & A*, L649.

448   Buck A.L., 1981. Research Manual (1996) updated equation from A.L. Buck, J. *Appl.*

449   *Meteorol.*, 20, 1527.

450   Chen N., Li G. Theoretical investigation on the inverse black body radiation problem.

451   *IEEE Trans Antennas and Propagation*, 1990, 38(8): 1287-1290.

452   Crovisier, J. et al., 2013. Observations of the 18-cm OH lines of Comet 103P/Hartley 2 at

453   Nancay in support to the EPOXI and Herschel missions. *Icarus*, 222, 679–683.

454   Dai X., Dai J. On unique existence theorem and exact solution formula of the inverse

455   black-body radiation problem. *IEEE Trans Antennas and Propagation*,1992,40(3):257-260.

456   Davidsson, B.J.R. et al., 2012. Thermal inertia and surface roughness of Comet

457   9P/Tempel 1. *Icarus*, 224, 154-171.

458   Davidsson, B.J.R. et al., 2015. Interpretation of thermal emission. I. The effect of

459   roughness for spatially resolved atmosphereless bodies. *Icarus*, 252, 1–21.

460   Davidsson, B.J.R. et al., 2022. Modelling the water and carbon dioxide production rates

461   of Comet 67P/Churyumov–Gerasimenko. *Monthly Notices of the Royal Astronomical Society*,

462   509, Issue 2, 3065-3085.

463   Davidsson, B.J.R., Gutierrez, P.J., Rickman, H., 2009. Physical properties of

464   morphological units on Comet 9P/Tempel 1 derived from near-IR Deep Impact spectra. *Icarus*,

465   201, 335–357.

466   De Sanctis et al., 2015. The diurnal cycle of water ice on comet 67P/Churyumov-

467   Gerasimenko. *Nature*, 525, 500-503.

468   Dello Russo, N. et al., 2011. The volatile composition and activity of comet 103P/Hartley

469   2 during the EPOXI closest approach. *Astrophys. J.*, 734, L8.

470   Fanale, F. P., & Salvail, J. R., 1984. An idealized short-period comet model: Surface

471   insolation, H2O flux, dust flux, and mantle evolution. *Icarus*, 60, 476-511.

472   Farnham, T.L. and Thomas, P.C., PLATE SHAPE MODEL OF COMET

473   103P/HARTLEY 2 V1.0, DIF-C-HRIV/MRI-5-HARTLEY2-SHAPE-V1.0, NASA Planetary

474   Data System, 2013.

475   Feistel, R. et al., 2007. Sublimation pressure and sublimation enthalpy of H2O ice Ih

476   between 0 and 273.16 K. *Geochimica et Cosmochimica Acta*, 71, 36 - 45.

477   Fornasier et al., 2016. Rosetta's comet 67P/Churyumov-Gerasimenko sheds its dusty

478   mantle to reveal its icy nature. *Science*, 23, 354(6319):1566-1570.

479   Fougere, N. et al., 2012. Understanding measured water rotational temperatures and

480   column densities in the very innermost coma of Comet 73P/Schwassmann–Wachmann 3B.

481   *Icarus*, 221, 174–185.

482   Gortsas et al., 2011. Thermal model of water and CO activity of Comet C/1995 O1 (Hale-

483   Bopp). *Icarus*, 212, 858-866.

484   Groussin, O. et al., 2004. The nuclei of comets 126P/IRAS and 103P/Hartley 2. *A&A*,
485 419, 375–383.

486   Groussin, O. et al., 2007. Surface temperature of the nucleus of Comet 9P/Tempel 1.
487 *Icarus*, 187, 16–25.

488   Groussin, O. et al., 2013. The temperature, thermal inertia, roughness and color of the
489 nuclei of Comets 103P/Hartley 2 and 9P/Tempel 1. *Icarus*, 222, 580–594.

490   Groussin, O. et al., 2019. The Thermal, Mechanical, Structural, and Dielectric Properties
491 of Cometary Nuclei After Rosetta. *Space Sci Rev*, (2019) 215:29.

492   Gutierrez et al., 2001. Effects of irregular shape and topography in thermophysical
493 models of heterogeneous cometary nuclei. *A&A*, 374, 326-336.

494   Hampton, D.L. et al., 2005. An overview of the instrument suite for the Deep Impact
495 mission. *Space Sci. Rev.*, 117, 43–93.

496   Handa, Y.P., et al., 1988. Energies of the phases of ice at low-temperature and pressure
497 relative to ice Ih. *Can J Chem*, 66(4):919–924.

498   Harker, D. E. et al., 2018. Hyperactivity and Dust Composition of Comet 103P/Hartley 2
499 During the EPOXI Encounter. *The Astronomical Journal*, 155, 199–211.

500   Harris, A.W., 1998. A thermal model for near-Earth asteroids. *Icarus*, 131, 291–301.

501   Herny et al., 2021. New constraints on the chemical composition and outgassing of
502 67P/Churyumov-Gerasimenko. *Planetary and Space Science*, L200.

503   Hu et al., 2017. Thermal modelling of water activity on comet 67P/Churyumov-
504 Gerasimenko with global dust mantle and plural dust-to-ice ratio. *MNRAS*, 469, S295–S311.

505   Huebner, W.F., 2006. Heat and Gas Diffusion in Comet Nuclei. *ISSI Science report*, SR-

506   004.

507   Ji, F. et al., 2006. A unified solution of the inverse black-body radiation problem ans

508   some exact solutions. *Inverse Problems*, 22, 1731-1737.

509   Ji, F. et al., 2011. A new solution method for black-body radiation inversion and the solar

510   area-temperature distribution. *Science China, Physics, Mechanics & Astronomy*, 54 (No.11),

511   2097-2112.

512   Julian, W.H. et al., 2000. Thermal Structure of Cometary Active Regions: Comet

513   1P/Halley. *Icarus*, 144, 160-171.

514   Keller, H.U. et al., 2015. The changing rotation period of comet 67P/Churyumov-

515   Gerasimenko controlled by its activity. *A&A*, 579, L5.

516   Kelly, M.S. et al., 2013. A distribution of large particles in the coma of Comet

517   103P/Hartley 2. *Icarus*, 222 (2): 634-652.

518   Kramers, H., 1951. The Sublimation of Ice in Vacuum. *Applied Scientific Research*, A3,

519   73–82.

520   Kührt, E., 1981. Temperature Profiles and Thermal Stresses in Cometary Nuclei. *Icarus*,

521   60, 512-521.

522   Lebofsky, L. A. et al., 1986. A refined "standard" thermal model for asteroids based on

523   observations of 1 Ceres and 2 Pallas. *Icarus*, 68, 239–251.

524   Li. J.et al., 2013. Photometric properties of the nucleus of Comet 103P/Hartley 2. *Icarus*,

525   222, 559–570.

526   McLaughlin, S.A., B. Carcich, S.E. Sackett, K.P. Klaasen, L.M. Feaga, and S. Protopapa,

527   EPOXI 103P/HARTLEY2 ENCOUNTER - HRII CALIBRATED SPECTRA V3.0, DIF-C-

528   HRII-3/4-EPOXI-HARTLEY2-V3.0, NASA Planetary Data System, 2014.

529   McMillan, J.A. et al., 1965. Vitreous ice - irreversible transformations during warm-up.

530   *Nature*, 206(4986):806–807.

531   Meech, K.J. et al., 2011. EPOXI: Comet 103P/Hartley 2 observations from a worldwide

532   campaign. *The Astrophysical Journal Letters*, 734: L1 (9pp).

533   Prialnik, 1989. Thermal evolution of cometary nuclei. *Advances in Space Research*, 9,

534   No.3, pp.25–40.

535   Protopapa, S. et al., 2014. Water ice and dust in the innermost coma of comet

536   103P/Hartley 2. *Icarus*, 238, 191–204.

537   Protopapa, S. et al., 2021. Non-detection of water-ice grains in the coma of comet

538   46P/Wirtanen and implications for hyperactivity. *The Planetary Science Journal*, June 2021.

539   Shi, X et al.,2016. Sunset jets observed on comet 67P/Churyumov-Gerasimenko

540   sustained by subsurface thermal lag. *A&A*, 586, A7.

541   Spencer, J.R., Lebofsky, L.A., Sykes, M.V., 1989. Systematic biases in radiometric

542   diameter determinations. *Icarus*, 78, 337–354.

543   Squires and Beard, 1961. Physical and orbital behavior of comets. *ApJ*, 163, 657-667.

544   Thomas, P.C. et al., 2013. Shape, density, and geology of the nucleus of Comet

545   103P/Hartley 2. *Icarus*, 222, 550–558.

546   Weaver, H. A. et al., 1994. Detection of CO Cameron band emission in comet P/Hartley

547   2 (1991 XV) with the Hubble Space Telescope. *The Astrophysical Journal*, 422, 374–380.

548   Weissman et al., 1981. Thermal modeling of cometary nuclei. *Icarus*, 47, 302–311.

549   Wesselink, A. J. et al., 1948. Heat conductivity and the nature of the lunar surface

550   material. *Bull. Astron. Inst. Neth.*, 10, 351–363.

551   Whipple, F. L, 1951. A Comet Model. II. Physical Relations for Comets and Meteors.

552   *The Astrophysical Journal*, 113, 464–474.

553   Yamamuro, O. et al., 1987. Heat-capacity and glass-transition of pure and doped cubic

554   ices. *J. Phys. Chem. Solids*, 48(10):935–942.

555   Yue, Y. et al., 2021. Dynamic Simulation and Parameter Fitting Method of Cometary

556   Dust Based on Machine Learning. *Experimental Astronomy*, 51, 391–424.